ACS APPLIED MATERIALS & INTERFACES

Letter

www.acsami.org

Ag Shell−Au Satellite Hetero-Nanostructure for Ultra-Sensitive, Reproducible, and Homogeneous NIR SERS Activity

Hyejin Chang,[†,‡] Homan Kang,[†,§,⊥] Jin-Kyoung Yang,[#] Ahla Jo,[∥] Ho-Young Lee,[∥] Yoon-Sik Lee,*[,§,#] and Dae Hong Jeong*[,‡,§]

[‡]Department of Chemistry Education, and [§]Interdisciplinary Program in Nano-Science and Technology, [#]School of Chemical and Biological Engineering, Seoul National University, Seoul 151-742, Republic of Korea

[∥]Department of Nuclear Medicine, Seoul National University Bundang Hospital, Seongnam 463-707, Republic of Korea

Supporting Information

ABSTRACT: It is critical to create isotropic hot spots in developing a reproducible, homogeneous, and ultrasensitive SERS probe. Here, an Ag shell−Au satellite (Ag−Au SS) nanostructure composed of an Ag shell and surrounding Au nanoparticles was developed as a near-IR active SERS probe. The heterometallic shell-satellite structure based SERS probe produced intense and uniform SERS signals (SERS enhancement factor ∼1.4 × 10^6 with 11% relative standard deviation) with high detectability (100% under current measurement condition) by 785 nm photoexcitation. This signal enhancement was independent of the laser polarizations, which reflects the isotropic feature of the SERS activity of Ag−Au SS from the three-dimensional (3D) distribution of SERS hot spots between the shell and the surrounding satellite particles. The Ag−Au SS nanostructure shows a great potential as a reproducible and quantifiable NIR SERS probe for in vivo targets.

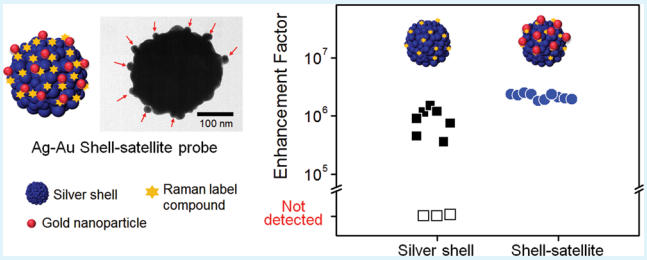

KEYWORDS: *core−satellite, surface-enhanced Raman scattering (SERS), SERS hot spot, near-infrared probe, uniform SERS activity*

Since in vitro and in vivo applicability of surface-enhanced Raman scattering (SERS) had been reported,[1−4] SERS probes have drawn much attention in multiplexed biodetection owing to their unique optical characteristics such as narrow bandwidth, high sensitivity, and no photobleaching.[5−9] To develop sensitive SERS probes, researchers have reported several approaches focusing on the synthesis of advanced nanostructures[10−18] or efficient Raman label compounds that are resonant with excitation light.[19−21] Especially, dimeric nanostructures[22−25] and small clusters[26,27] were reported as SERS probes. These nanostructures could generate hot spots from nanogap junctions between nanoparticles (NPs) where the electromagnetic field is significantly concentrated, allowing for an ultrasensitive SERS signal.[14,28,29] However, the anisotropic structure with uncontrollable nanogap junctions leads to signal fluctuation and dependency on incident light polarization. Therefore, for developing reproducible and homogeneous SERS probes, creating and controlling hot spots in isotropic structures is a critical issue.[15,16]

Recently, a highly uniform and reproducible SERS probe in the visible range was reported by Lim et al.[13] It is worth noting that signal fluctuations among SERS probes were minimal because the 1 nm gap in the interior of the SERS probe was precisely controlled by utilizing single-stranded DNA. In addition, three-dimensional (3D) core−satellite type assembled SERS nanoprobes with a uniform signal have been reported.[10−12,16,18,30,31] However, these nanosphere-based nanogap structures and 3D NP-assemblies are still limited for use in vivo applications because of their plasmonic resonance in the visible optical range where animal tissue has large absorption and autofluorescence. Therefore, the SERS probes which are sensitive in the near-Infrared (NIR) region, the so-called biological window, for effective in vivo detection and imaging of biological targets need to be developed.[17,32−34]

Herein, we demonstrate an NIR-sensitive heteronanostructure as a SERS probe which has a strong and highly uniform SERS activity. This NIR SERS probe consists of an Ag shell and Au NP satellites (Ag−Au SS). The plasmonic resonance is red-shifted to the NIR region with additional enhancements, enabling the detection even at a single probe level. The Ag−Au SS probe is 100% detectable under 785 nm photoexcitation because of multiple SERS hot spots, which were designed to generate reproducible and isotropic SERS activity.

Fabrication details of Ag−Au SS probes are illustrated in Figure 1. We utilized a solid support and selective desorption method[16] to prevent NPs' aggregations during synthesis and for easy separation of assembled nanoparticles and nonassembled nanoparticles. First, amine-functionalized silicon wafer was immersed into the Ag shell colloidal solution for 3 h (Figure 1a). The Ag shell (251 ± 16 nm in diameter, ca. 50 nm of shell thickness) was synthesized by using a one-step method.[35] It has

Received: June 11, 2014
Accepted: July 31, 2014
Published: July 31, 2014

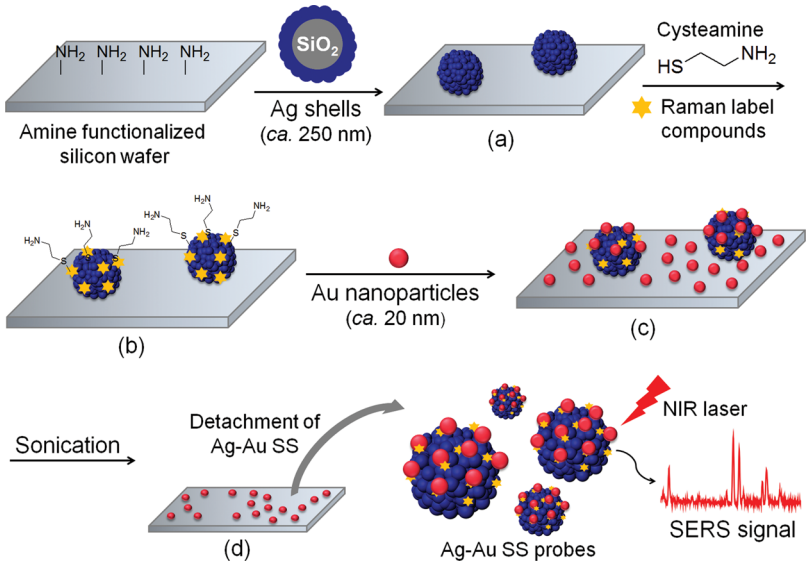

Figure 1. Schematic illustration for the fabrication of Ag shell–Au satellite (Ag–Au SS) probes on solid substrate. (a) Ag shells are immobilized on the amine-functionalized silicon wafer through electrostatic interactions. (b) Cysteamine (a linker molecule) and Raman label compound are adsorbed on the surface of Ag shells. (c) Au NPs as satellites were introduced electrostatically onto Ag shells on a silicon wafer. (d) Ag–Au SS probes were selectively detached from the silicon wafer by moderate sonication.

dielectric silica core and broad range surface plasmonic bands. The Ag shell facilitates the development of the NIR-active probes owing to the intrinsic SERS activity of the Ag shell in the NIR region. After the attachment of Ag shells on the silicon wafer, a Raman label compound (4 mM in ethanol) and cysteamine (2 mM in ethanol) as a linker molecule were coadsorbed on the surface of the Ag shell by dipping the silicon wafer in Raman label compound and cysteamine mixed solution for 1 h (Figure 1b). Cysteamine is a well-known cross-linker molecule that can provide structural stability of nanoassemblies by forming a monolayer on the metal surface via chemisorption with the thiol group, and attaching another substances with the amine group.[36] Next, the citrate-capped Au NPs (ca. 20 nm) were immobilized on the surface of the amine functionalized Ag shell and silicon wafer (Figure 1c). Finally, the Ag–Au SS probe adsorbed silicon wafer was sonicated in ethanol for 1 min, leading to the selective detachment of Ag–Au SS probes from the silicon wafer into the ethanol because of the different desorption efficiency depending on the particle size (Figure 1d, and Figure S1 in the Supporting Information).[16]

The samples during the fabrication process were characterized by scanning electron microscopy (SEM), transmission electron microscopy (TEM), and energy-dispersive X-ray spectroscopy (EDX) measurements (Figure 2). Before detachment of the Ag–Au SS probes from the silicon wafer, the formation of Ag shell–Au satellite structures was confirmed by SEM (Figure 2a) and EDX analysis (Figure 2b–e). From the SEM image, it was confirmed that Au NPs were successfully immobilized on the surface of Ag shells as well as on that of the silicon wafer. The number of Au satellite NPs per Ag shell was estimated to be 21 ± 4 on average by counting the Au satellite NPs on the observable side from 60 Ag–Au SS probe particles. In addition, the elemental mapping images clearly show that both the Ag atoms and the Au atoms are well-distributed throughout the core part, indicating that the Ag–Au heterometallic structure was successfully assembled.

Next, the morphology and optical properties of the detached Ag–Au SS probes were confirmed. The Au NPs existing on the surface of the Ag shell were clearly observed as shown in Figure 2f (red arrows indicate satellite Au NPs), compared with the TEM image of the Ag shell (see Figure S2 in the Supporting Information). This result proves that the Ag–Au SS structure is maintained during the detachment process. Furthermore, the UV–vis–NIR extinction spectra of Ag–Au SS probes (λ_{max} = 698 nm) demonstrate that their surface plasmon band was red-shifted from that of the individual Ag shell (λ_{max} = 620 nm) and Au NPs (λ_{max} = 520 nm) (Figure 2h). This red-shifted plasmon resonance band is attributed to the strong plasmon coupling between the Ag shell and Au NPs (less than 1 nm gap, Figure 2g),[37] affording Ag–Au SS probes a plasmon coupling band in the NIR region.

To evaluate the Ag–Au SS probe as the NIR sensitive SERS probe, the SERS spectra of single probes were obtained with three different excitation lines (532, 647, and 785 nm). Raman measurements were performed by point-by-point mapping with a 1 μm step size under the appropriate condition depending on the excitation wavelengths. Subsequently, SEM images were compared with the corresponding Raman maps to ensure the existence of single particles. Figure 3a shows typical SERS spectrum of an Ag–Au SS probe coded with 4-fluorobenzenethiol obtained by 785 nm photoexcitation (28 μW) and 10 s acquisition. SERS intensity map of the 1075 cm^{-1} band from Ag–Au SS probes dispersed on silicon wafer is drawn overlaid with its corresponding SEM image (Figure 3b). SERS enhancement factors (EFs) and percentages of detectable single particles for three different excitation lines were estimated for the Ag–Au SS probe and for the Ag shell as comparison (Figure 3c and Table S1 in the Supporting Information). Interestingly, two notable features were found from this result. First, the SERS EF values of Ag–Au SS probe exhibit 4.1-fold (532 nm), 3.1-fold (647 nm), and 2.5-fold (785 nm) increases compared with those of Ag shells. Although the bumpy surface of the Ag shell induces an electromagnetic field enhancement, the interparticle gaps in the shell-satellite structure can provide further enhancement, producing a highly concentrated electromagnetic field.[28] Especially, the Ag–Au SS

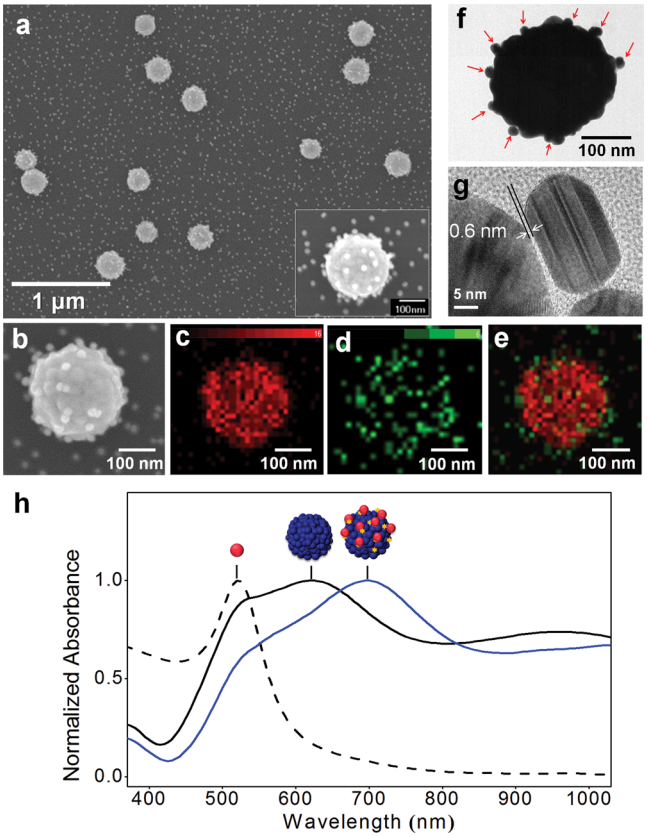

Figure 2. Structural and optical characteristics of Ag–Au SS probes. (a) SEM image of the Ag–Au SS probes fabricated on a silicon wafer. (b) Highly magnified SEM image of one Ag–Au SS probe and its EDX maps showing the elemental distributions of (c) Ag from L_{α}, (d) Au from M_{α}, and (e) merged image of Ag and Au. (f) TEM image of the Ag–Au SS probe. (g) HR-TEM image of Ag shell-to-Au satellite interparticle gap. The two arrows indicate the subnanometer gap. (h) UV–visible–NIR extinction spectra of Au NPs (black dashed line, λ_{max} = 520 nm), Ag shells (black solid line, λ_{max} = 620 nm), and Ag–Au SS probes (blue solid line, λ_{max} = 698 nm).

probe exhibited the highest EF value (1.4×10^6 on average) for NIR excitation (785 nm) among the three laser lines. Second, the detectability of Ag–Au SS probes was increased remarkably compared with that of the Ag shell, reaching up to 100% in the case of NIR excitation (785 nm). In addition, the distributions of EF values from the Ag–Au SS probes were highly uniform, which is attributed to the multiple hot spots produced by the shell–satellite structure. This feature refers to "reproducibility" of SERS intensity over probe particles, of which concept follows the previously reported article showing the degree of the particle-to-particle signal distribution.[13]

Another aspect is "reproducibility" of SERS intensity irrespective of incident laser polarization. To confirm whether or not the signal uniformity of Ag–Au SS probe is isotropic over incident laser polarization, SERS spectra of an Ag–Au SS probe were obtained using a 785 nm laser, of which the polarization was rotated in three directions. As shown in Figure 4, the 4-FBT signals of the Ag–Au SS probe were consistent when the laser polarization was rotated by 45° and 90° away from the onset axis. On the contrary, because of the polarization properties, the SERS signals from the dimers have vanished when the excitation laser is polarized orthogonal to the longitudinal axis.[25,38] In addition, for proving the other reproducibility, the photostability of Ag–Au SS probes was

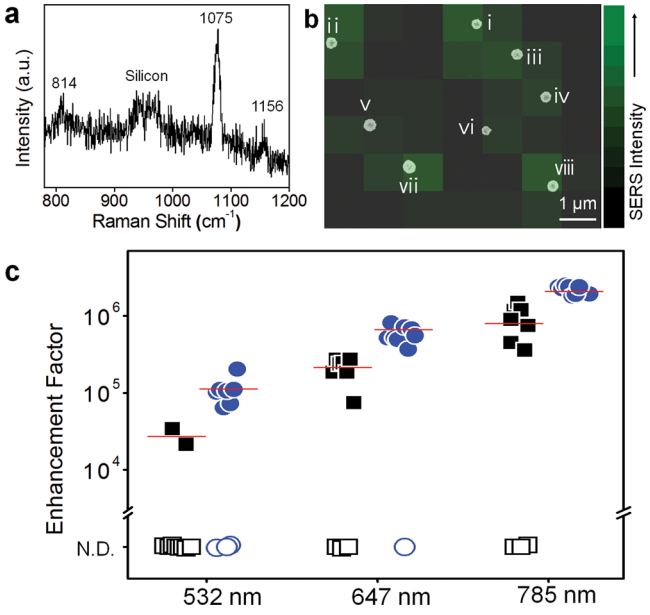

Figure 3. Analysis of SERS enhancement of Ag–Au SS probes by single probe particle characterization. (a) Representative SERS spectrum of an Ag–Au SS probe coded with 4-fluorobenzenethiol obtained by 785 nm photoexcitation (28 μW) and 10 s acquisition. (b) SERS intensity map of the 1075 cm^{-1} band from Ag–Au SS probes dispersed on silicon wafer. The SERS intensity map was overlaid with its corresponding SEM image. Enhancement factor of each Ag–Au SS probe on the silicon substrate at 785 nm photoexcitation is (i) 1.6×10^6, (ii) 1.5×10^6, (iii) 1.4×10^6, (iv) 1.1×10^6, (v) 1.1×10^6, (vi) 1.0×10^6, (vii) 1.2×10^6, and (viii) 1.5×10^6. (c) Enhancement factors of Ag shells (black solid squares) and Ag–Au SS probes (blue solid circles) at three different excitation wavelengths (532, 647, and 785 nm). All empty dots indicate undetectable particles. The Ag–Au SS probes exhibit higher enhancement factor values than the Ag shell NPs in each excitation line. The Ag–Au SS probes exhibit the highest detectability under the NIR excitation laser (100% detectable with 785 nm photoexcitation).

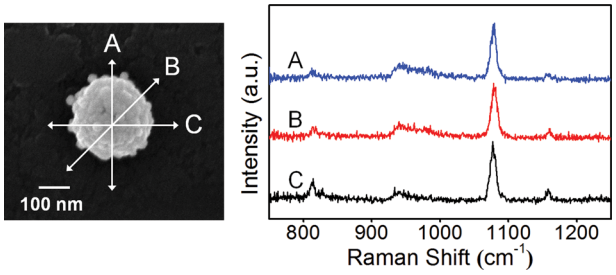

Figure 4. SERS spectra obtained from Ag–Au SS probe with different orientations relative to the polarization of the excitation laser. The 4-FBT signals from the Ag–Au SS probe are consistent when the laser polarizations are rotated by (B) 45° and (C) 90° away from (A) the onset axis. All spectra were taken using a 785 nm photoexcitation (180 μW at the sample) and 10 s acquisition time.

tested over irradiation time. We obtained the SERS spectra from thesingle Ag–Au SS particle while irradiating laser lights for approximately 100 s. Each spectrum was obtained with 5-s acquisition (see Figure S5a in the Supporting Information). The signal intensities exhibited little decrease indicating that Au–Ag SS probe is stable under laser exposure (see Figure S5b in the Supporting Information). These results reveal that the Ag–Au SS probes are a robust platform for highly reproducible

dx.doi.org/10.1021/am503675x | ACS Appl. Mater. Interfaces 2014, 6, 11859–11863

SERS analysis because of the multiple hot spots and the red-shifted plasmonic resonance.

To expand the utility of Ag−Au SS probe, we prepared two types of Ag−Au SS probes by using different Raman label compounds such as 4-chlorobenzenethiol (4-CBT), and 4-bromobenzenethiol (4-BBT). Each type of Ag−Au SS probe has distinctive spectral fingerprint and exhibits strong single-particle SERS activities, suggesting that these Ag−Au SS probes can be used in multiplexed analysis (see Figure S4 in the Supporting Information).

Finally, to demonstrate the potential applicability of Ag−Au SS as NIR SERS probe, a proof-of-concept experiment was performed in a mouse model. As shown in Figure 5a, a 10 μL

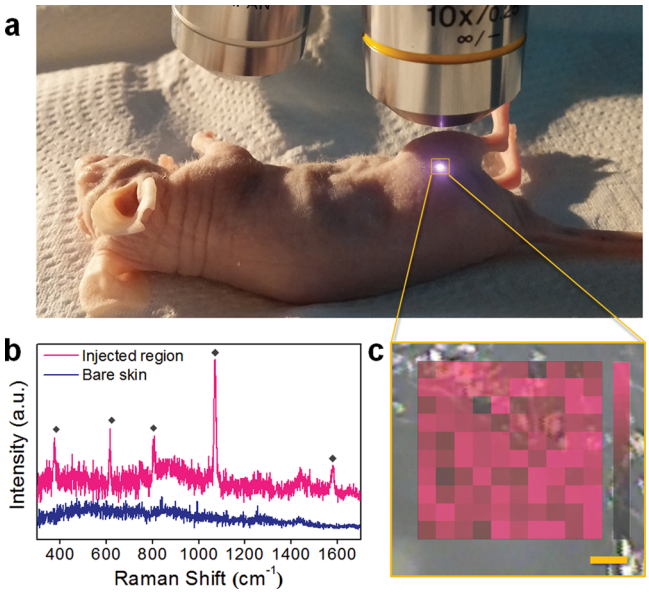

Figure 5. In vivo SERS detection using Ag−Au SS probes. (a) Photograph of Raman measurement setup for in vivo detection. (b) SERS spectra obtained from mouse skin with Ag−Au SS probes injected and without injected by the 785 nm photoexcitation of 43 mW laser power and 120 s acquisition time. (c) SERS intensity map of the 1075 cm^{-1} band of Ag−Au SS probes at the injected region. The mapping is 100 × 100 μm^2, which was scanned at 10 μm interval. The scale bar is 20 μm.

aliquot of Ag−Au SS probe labeled with 4-FBT was subcutaneously injected at gluteal region of a nude mouse, and the SERS spectra were obtained using a Raman system with a 785 nm photoexcitation. The injected region exhibited the SERS signal which is well matched with the spectrum of 4-FBT-labeled Ag−Au SS probe, and no distinctive Raman signal could be observed from normal skin region (Figure 5b). The intensity map of the 1075 cm^{-1} band exhibits that strong Raman signals of Ag−Au SS probes were easily detected in the probe injected region (Figure 5c). These results strongly suggest that the Ag−Au SS probes can be used for a sensitive detection of target biomolecules in vivo.

In summary, we developed a heterometallic SERS probe based on a Ag shell and Au NPs, affording highly uniform and strong SERS activity. The Ag−Au SS structures exhibited a red-shift of plasmonic resonance band to the NIR region with highly enhanced SERS signals (SERS enhancement factor: ∼1.4 × 10^6 with 11% relative standard deviation) and high detectability (100% under our measurement condition) by the 785 nm photoexcitation. These outstanding SERS activities were independent of the laser polarizations and largely attributed to the 3D distribution of SERS hot spots between the Ag shell and the satellite particles on it. Finally, we demonstrated Ag−Au SS as NIR SERS probes through proof-of-concept of in vivo imaging application. The novel properties of SERS probes in the NIR optical window have potential valuables for applications in in vivo bio analysis.

■ ASSOCIATED CONTENT

Supporting Information

Experimental details, SEM images for comparison of different desorption efficiencies and purification, SERS intensity mappings for single particle detection, and table for comparison of single particle SERS activity. This material is available free of charge via the Internet at http://pubs.acs.org.

■ AUTHOR INFORMATION

Corresponding Authors

*E-mail: jeongdh@snu.ac.kr.

*E-mail: yslee@snu.ac.kr

Present Address

⊥H.K. is currently at School of Electrical Engineering and Computer Science, Seoul National University, Seoul 151−742, Republic of Korea.

Author Contributions

†Authors H.C. and H.K. contributed equally.

Notes

The authors declare no competing financial interest.

■ ACKNOWLEDGMENTS

This research was supported by the Pioneer Research Center Program through the National Research Foundation of Korea, funded by the Ministry of Science, ICT & Future Planning (Grant 2013-006163) and a grant of the Korean Health Technology R&D Project, Ministry of Health & Welfare (HI13C-1299-010013).

■ REFERENCES

(1) Keren, S.; Zavaleta, C.; Cheng, Z.; de la Zerda, A.; Gheysens, O.; Gambhir, S. S. Noninvasive Molecular Imaging of Small Living Subjects Using Raman Spectroscopy. *Proc. Natl. Acad. Sci. U.S.A.* **2008**, *105*, 5844−5849.

(2) Stuart, D. A.; Yuen, J. M.; Shah, N.; Lyandres, O.; Yonzon, C. R.; Glucksberg, M. R.; Walsh, J. T.; Van Duyne, R. P. In vivo Glucose Measurement by Surface-Enhanced Raman Spectroscopy. *Anal. Chem.* **2006**, *78*, 7211−7215.

(3) Qian, X.; Peng, X. H.; Ansari, D. O.; Yin-Goen, Q.; Chen, G. Z.; Shin, D. M.; Yang, L.; Young, A. N.; Wang, M. D.; Nie, S. In Vivo Tumor Targeting and Spectroscopic Detection with Surface-Enhanced Raman Nanoparticle Tags. *Nat. Biotechnol.* **2008**, *26*, 83−90.

(4) Ni, J.; Lipert, R. J.; Dawson, G. B.; Porter, M. D. Immunoassay Readout Method Using Extrinsic Raman Labels Adsorbed on Immunogold Colloids. *Anal. Chem.* **1999**, *71*, 4903−4908.

(5) Alvarez-Puebla, R. A.; Liz-Marzán, L. M. SERS-Based Diagnosis and Biodetection. *Small* **2010**, *6*, 604−610.

(6) Schlücker, S. SERS Microscopy: Nanoparticle Probes and Biomedical Applications. *ChemPhysChem* **2009**, *10*, 1344−1354.

(7) Jun, B. H.; Kim, G.; Noh, M. S.; Kang, H.; Kim, Y. K.; Cho, M. H.; Jeong, D. H.; Lee, Y. S. Surface-Enhanced Raman Scattering-Active Nanostructures and Strategies for Bioassays. *Nanomedicine* **2011**, *6*, 1463−1480.

(8) Lim, C.; Hong, J.; Chung, B. G.; deMello, A. J.; Choo, J. Optofluidic Platforms Based on Surface-Enhanced Raman Scattering. *Analyst* **2010**, *135*, 837−844.

(9) Moskovits, M. Surface-enhanced spectroscopy. *Rev. Mod. Phys.* **1985**, *57*, 783−826.
(10) Gandra, N.; Abbas, A.; Tian, L.; Singamaneni, S. Plasmonic Planet-Satellite Analogues: Hierarchical Self-Assembly of Gold Nanostructures. *Nano Lett.* **2012**, *12*, 2645−2651.
(11) Gandra, N.; Singamaneni, S. "Clicked" Plasmonic Core-Satellites: Covalently Assembled Gold Nanoparticles. *Chem. Commun.* **2012**, *48*, 11540−11542.
(12) Gellner, M.; Steinigeweg, D.; Ichilmann, S.; Salehi, M.; Schütz, M.; Kompe, K.; Haase, M.; Schlücker, S. 3D Self-Assembled Plasmonic Superstructures of Gold Nanospheres: Synthesis and Characterization at the Single-Particle Level. *Small* **2011**, *7*, 3445−3451.
(13) Lim, D. K.; Jeon, K. S.; Hwang, J. H.; Kim, H.; Kwon, S.; Suh, Y. D.; Nam, J. M. Highly Uniform and Reproducible Surface-Enhanced Raman Scattering from DNA-Tailorable Nanoparticles with 1-nm Interior Gap. *Nat. Nanotechnol.* **2011**, *6*, 452−460.
(14) Lim, D. K.; Jeon, K. S.; Kim, H. M.; Nam, J. M.; Suh, Y. D. Nanogap-Engineerable Raman-Active Nanodumbbells for Single-Molecule Detection. *Nat. Mater.* **2010**, *9*, 60−67.
(15) Mulvihill, M. J.; Ling, X. Y.; Henzie, J.; Yang, P. Anisotropic Etching of Silver Nanoparticles for Plasmonic Structures Capable of Single-Particle SERS. *J. Am. Chem. Soc.* **2010**, *132*, 268−274.
(16) Yoon, J. H.; Lim, J.; Yoon, S. Controlled Assembly and Plasmonic Properties of Asymmetric Core-Satellite Nanoassemblies. *ACS Nano* **2012**, *6*, 7199−7208.
(17) Rodriguez-Lorenzo, L.; Alvarez-Puebla, R. A.; de Abajo, F. J. G.; Liz-Marzan, L. M. Surface Enhanced Raman Scattering Using Star-Shaped Gold Colloidal Nanoparticles. *J. Phys. Chem. C* **2010**, *114*, 7336−7340.
(18) Xu, L.; Kuang, H.; Xu, C.; Ma, W.; Wang, L.; Kotov, N. A. Regiospecific Plasmonic Assemblies for In Situ Raman Spectroscopy in Live Cells. *J. Am. Chem. Soc.* **2012**, *134*, 1699−1709.
(19) Cho, S. J.; Ahn, Y. H.; Maiti, K. K.; Dinish, U. S.; Fu, C. Y.; Thoniyot, P.; Olivo, M.; Chang, Y. T. Combinatorial Synthesis of a Triphenylmethine Library and Their Application in the Development of Surface Enhanced Raman Scattering (SERS) Probes. *Chem. Commun.* **2010**, *46*, 722−724.
(20) Samanta, A.; Maiti, K. K.; Soh, K.-S.; Liao, X.; Vendrell, M.; Dinish, U. S.; Yun, S.-W.; Bhuvaneswari, R.; Kim, H.; Rautela, S.; Chung, J.; Olivo, M.; Chang, Y.-T. Ultrasensitive Near-Infrared Raman Reporters for SERS-Based In Vivo Cancer Detection. *Angew. Chem., Int. Ed.* **2011**, *123*, 6213−6216.
(21) Samanta, A.; Jana, S.; Das, R. K.; Chang, Y.-T. Wavelength and Shape Dependent SERS Study to Develop Ultrasensitive Nanotags for Imaging of Cancer Cells. *RSC Adv.* **2014**, *4*, 12415−12421.
(22) Braun, G. B.; Lee, S. J.; Laurence, T.; Fera, N.; Fabris, L.; Bazan, G. C.; Moskovits, M.; Reich, N. O. Generalized Approach to SERS-active Nanomaterials via Controlled Nanoparticle Linking, Polymer Encapsulation, and Small-Molecule Infusion. *J. Phys. Chem. C* **2009**, *113*, 13622−13629.
(23) Guarrotxena, N.; Liu, B.; Fabris, L.; Bazan, G. C. Antitags: Nanostructured Tools for Developing SERS-Based ELISA Analogs. *Adv. Mater.* **2010**, *22*, 4954−4958.
(24) Guerrini, L.; Graham, D. Molecularly-Mediated Assemblies of Plasmonic Nanoparticles for Surface-Enhanced Raman Spectroscopy Applications. *Chem. Soc. Rev.* **2012**, *41*, 7085−7107.
(25) Li, W. Y.; Camargo, P. H. C.; Lu, X. M.; Xia, Y. N. Dimers of Silver Nanospheres: Facile Synthesis and Their Use as Hot Spots for Surface-Enhanced Raman Scattering. *Nano Lett.* **2009**, *9*, 485−490.
(26) Brown, L. O.; Doorn, S. K. A Controlled and Reproducible Pathway to Dye-Tagged, Encapsulated Silver Nanoparticles as Substrates for SERS Multiplexing. *Langmuir* **2008**, *24*, 2277−2280.
(27) Yigit, M. V.; Zhu, L.; Ifediba, M. A.; Zhang, Y.; Carr, K.; Moore, A.; Medarova, Z. Noninvasive MRI-SERS Imaging in Living Mice Using an Innately Bimodal Nanomaterial. *ACS Nano* **2011**, *5*, 1056−1066.
(28) Lal, S.; Link, S.; Halas, N. J. Nano-optics from Sensing to Waveguiding. *Nat. Photonics* **2007**, *1*, 641−648.
(29) Fang, Y.; Seong, N. H.; Dlott, D. D. Measurement of the Distribution of Site Enhancements in Surface-Enhanced Raman Scattering. *Science* **2008**, *321*, 388−392.
(30) Chen, S.-Y.; Lazarides, A. A. Quantitative Amplification of Cy5 SERS in 'Warm Spots' Created by Plasmonic Coupling in Nanoparticle Assemblies of Controlled Structure. *J. Phys. Chem. C* **2009**, *113*, 12167−12175.
(31) Xu, L.; Hao, C.; Yin, H.; Liu, L.; Ma, W.; Wang, L.; Kuang, H.; Xu, C. Plasmonic Core−Satellites Nanostructures with High Chirality and Bioproperty. *J. Phys. Chem. Lett.* **2013**, *4*, 2379−2384.
(32) Kang, H.; Jeong, S.; Park, Y.; Yim, J.; Jun, B.-H.; Kyeong, S.; Yang, J.-K.; Kim, G.; Hong, S.; Lee, L. P.; Kim, J.-H.; Lee, H.-Y.; Jeong, D. H.; Lee, Y.-S. Near-Infrared SERS Nanoprobes with Plasmonic Au/Ag Hollow-Shell Assemblies for In Vivo Multiplex Detection. *Adv. Funct. Mater.* **2013**, *23*, 3719−3727.
(33) Ghosh, D.; Lee, Y.; Thomas, S.; Kohli, A. G.; Yun, D. S.; Belcher, A. M.; Kelly, K. A. M13-templated Magnetic Nanoparticles for Targeted In Vivo Imaging of Prostate Cancer. *Nat. Nanotechnol.* **2012**, *7*, 677−682.
(34) Smith, B. R.; Zavaleta, C.; Rosenberg, J.; Tong, R.; Ramunas, J.; Liu, Z.; Dai, H.; Gambhir, S. S. High-Resolution, Serial Intravital Microscopic Imaging of Nanoparticle Delivery and Targeting in a Small Animal Tumor Model. *Nano Today* **2013**, *8*, 126−137.
(35) Kang, H.; Yang, J.-K.; Noh, M. S.; Jo, A.; Jeong, S.; Lee, M.; Lee, S.; Chang, H.; Lee, H.; Jeon, S.-J.; Kim, H.-I.; Cho, M.-H.; Lee, H.-Y.; Kim, J.-H.; Jeong, D. H.; Lee, Y.-S. One-Step Synthesis of Silver Nanoshell with Bumps for Highly Sensitive Near-IR SERS Nanoprobes. *J. Mater. Chem. B* **2014**, *2*, 4415−4421.
(36) Abbas, A.; Tian, L.; Kattumenu, R.; Halim, A.; Singamaneni, S. Freezing the Self-Assembly Process of Gold Nanocrystals. *Chem. Commun.* **2012**, *48*, 1677−9.
(37) Yoon, J. H.; Zhou, Y.; Blaber, M. G.; Schatz, G. C.; Yoon, S. Surface Plasmon Coupling of Compositionally Heterogeneous Core−Satellite Nanoassemblies. *J. Phys. Chem. Lett.* **2013**, *4*, 1371−1378.
(38) Steinigeweg, D.; Schütz, M.; Schlücker, S. Single Gold Trimers and 3D Superstructures Exhibit a Polarization-Independent SERS Response. *Nanoscale* **2013**, *5*, 110−113.